Rationalizing the Extent of the "Sergeants-and-Soldiers" Effect in Supramolecular Helical Catalysts: Effect of Copper Coordination

Ahmad Hammoud, Yan Li, Mayte Martínez-Aguirre, Huanjun Kong, Ludovic Dubreucq, Claire Troufflard, Laurent Bouteiller, Matthieu Raynal

Chemistry Europe
European Chemical Societies Publishing

WILEY VCH

Excellence in Chemistry Research

Announcing our new flagship journal

- Gold Open Access
- Publishing charges waived
- Preprints welcome
- Edited by active scientists

Meet the Editors of *ChemistryEurope*

Luisa De Cola
Università degli Studi di Milano Statale, Italy

Ive Hermans
University of Wisconsin-Madison, USA

Ken Tanaka
Tokyo Institute of Technology, Japan

Chemistry–A European Journal
Research Article
doi.org/10.1002/chem.202300189
Chemistry Europe
European Chemical Societies Publishing
www.chemeurj.org

Rationalizing the Extent of the "Sergeants-and-Soldiers" Effect in Supramolecular Helical Catalysts: Effect of Copper Coordination

Ahmad Hammoud,[a] Yan Li,[a] Mayte A. Martínez-Aguirre,[a] Huanjun Kong,[a] Ludovic Dubreucq,[a] Claire Troufflard,[a] Laurent Bouteiller,[a] and Matthieu Raynal*[a]

Abstract: Aggregation of supramolecular helices, for example through interdigitation of their alkyl side chains or through more directional supramolecular interactions, leads to hierarchical architectures with original structural and chiroptical properties. However, when a chiral monomer (the "sergeant") is introduced as a minor component in these assemblies composed of a majority of achiral monomers (the "soldiers"), it is not clear how the aggregation changes the ability of the sergeant to induce a preferential helicity to the polymer main chain (the so-called "sergeants-and-soldiers" effect). This study reports a detailed investigation of the influence of $[Cu(OAc)_2{\cdot}H_2O]$ coordination on the structure and chiroptical properties of helical hydrogen-bonded co-assemblies composed of a catalytically-active benzene-1,3,5-tricarboxamide (BTA) monomer, acting as the "soldier", and an enantiopure BTA monomer derived from cyclohexylalanine, playing the role of the "sergeant". The copper actually significantly influences the extent of the "sergeants-and-soldiers" effect since it acts as a crosslink that induces some chiral defects in the supramolecular helices. These crosslinks appear to be preserved during the catalytic hydrosilylation of 4-nitroacetophenone. The aggregation of helices through the formation of copper crosslinks is reversible since homochiral single helices are exclusively formed in the case of sergeant-rich assemblies. The fact that both main chain and side chain aggregation affects the chiroptical properties of supramolecular helices must be considered in the design of elaborated chiral materials.

Introduction

Non-linear effects,[1,2] asymmetric auto-replication,[3] and additive Horeau amplification of enantioselectivity[4] all refer to an enhancement of the optically purity of small molecules relatively to expectations, and as such, their implication in the emergence of biological homochirality is attractive, even though speculative yet.[5,6] Taming the chiral nature of macromolecules offers another angle to tackle the challenging question of the origin of homochiral nature of biopolymers as well as to construct innovative chiral materials.[7] The possibility of controlling the configuration adopted by synthetic covalent polymers by means of sense-selective[8] and stereospecific[9] polymerization is well-established but the use of chiral monomers as inducers appears to be more modular.[10] Randomly polymerized achiral and chiral monomers, with the latter in minority, lead to helical polymers with "disproportionally large optical purities",[11] a phenomenon originally discovered in the sixties[12,13] and later on characterized on poly(isocyanate) by M. Green as the "sergeants-and-soldiers" (S&S) effect.[14] The ability of the chiral monomers, the "sergeants", to induce a preferred helical configuration to polymers composed in majority of achiral monomers (the "soldiers") is particularly strong in macromolecules for which helix reversals and mismatch defects appear to exchange dynamically along the polymer main chain. It is worth noting here that in their seminal papers, Green and co-workers already reported that experimental parameters such as the nature of the solvent and the temperature may have a drastic effect on the extent of S&S effect, even though the origin of these perturbations were hard to correlate.[14,15] Since then, the S&S effect has been found to be operative, typically in the range of a few percent of "sergeants", in various covalent[10] and supramolecular polymers,[7,16] and has been exploited towards numerous chirality-driven applications, for example selective emission[17–21] or reflection[22] of CPL, chirality-induced spin-selective systems[23] and asymmetric catalysts.[24–26]

S&S-type supramolecular polymers assembled from chiral and achiral monomers with a disc-like shape, such as benzene-1,3,5-tricarboxamides (BTAs) and their analogues with different central cores, have been particularly studied.[27–29] The helical structure, supported by a threefold hydrogen-bonded network, is particularly sensitive to small chiral biases and thus constitutes a suitable platform to probe the chiroptical proper-

[a] Dr. A. Hammoud, Dr. Y. Li, Dr. M. A. Martínez-Aguirre, H. Kong, L. Dubreucq, C. Troufflard, Dr. L. Bouteiller, Dr. M. Raynal
Sorbonne Université, CNRS
Institut Parisien de Chimie Moléculaire
Equipe Chimie des Polymères
4 Place Jussieu, 75005 Paris (France)
E-mail: matthieu.raynal@sorbonne-universite.fr

Supporting information for this article is available on the WWW under https://doi.org/10.1002/chem.202300189

ties of S&S-type coassemblies both experimentally[30–34] and theoretically.[35,36] Meijer and co-workers notably found that lowering the temperature increases the extent of the S&S effect of BTA coassemblies by increasing the mismatch penalty value.[34] In addition to the temperature,[34,37–39] parameters investigated to tune the S&S effect include the chemical nature of the "sergeants"[34,37–43] or the "soldiers",[41] the concentration,[34] the solvent,[44,45] a physical field,[46] and additives.[47,48] The extent of the S&S effect is correlated to the number of defects, as quantified by the energetic values associated with helix reversals and chiral mismatches.[49,50] Aggregation of hydrogen-bonded helical structures by complementary interactions has been exploited to construct hierarchical[39,40,51–53] or competitive[54] supramolecular aggregates with tunable chiroptical properties. The orthogonality of hydrogen bonding and metal-ligand interactions also allowed the construction of crosslinked supramolecular polymer networks, yet the impact of chirality was not probed in this system.[55] Overall, it is not clear how the chiral induction ability of the "sergeant" is affected by the aggregation process. As lateral aggregation of supramolecular polymers can be achieved by various mechanisms, such as van der Waals or directional metal-ligand interactions between polymer side chains, it would be interesting to probe and rationalize the influence of aggregation on the extent of the S&S effect in hydrogen-bonded helices.

Our group investigated S&S-type helical coassemblies composed of an achiral BTA phosphine ligand (the "soldier") and an enantiopure BTA derived from amino ester (the "sergeant") as scaffold for asymmetric rhodium-[56,57] and copper-catalyzed reactions.[58–61] When a sufficient amount of "sergeant" is incorporated into the assemblies, homochiral helices are generated that yield the optimal selectivity for the catalytic system under consideration. We actually found that the enantioselectivity of the copper-catalyzed hydrosilylation of 4-nitroacetophenone (NPnone) is linearly related to the optical purity of the helices coordinated to $[Cu(OAc)_2{\cdot}H_2O]$, as probed by circular dichroism (CD) spectroscopy.[60] This means that for a given S&S combination, the selectivity of the reaction can in principle be predicted by a single CD measurement. Screening of S&S-type mixtures can be envisaged, and it is thus important to elucidate whether copper has an impact on the extent of chirality induction. Previously, we found no significant influence of $[Cu(OAc)_2{\cdot}H_2O]$ on the structure of S&S-type co-assemblies embedding a large fraction of "sergeants".[59] In this work, the structure and chiroptical properties of copper-bound and copper-free S&S-type helices composed of **BTA P** and **BTA Cha** (Scheme 1) were precisely assessed by CD, Fourier-Transform Infrared (FTIR), Nuclear Magnetic Resonance (NMR), UV-Vis and Small-Angle Neutron Scattering (SANS) analyses and correlated to the selectivity obtained in the hydrosilylation of NPnone. These analyses actually reveal a more complex picture: The S&S effect is indeed drastically influenced by the presence of copper, since copper sites act as crosslinks between the helical stacks. The competition between aggregated and non-aggregated helices is shifted towards homochiral single helices for "sergeant"-rich helices.

Results

Chiroptical properties of S&S-type assemblies with and without [Cu]

BTA Cha was selected as the "sergeant" given its propensity to intercalate efficiently into the stacks formed by **BTA P** as represented in Scheme 1.[60] S&S-type co-assemblies without [Cu] are prepared by directly mixing **BTA P** and one of the BTA Cha enantiomer in toluene. S&S-type co-assemblies with [Cu] are prepared in two steps by firstly complexing **BTA P** and $[Cu(OAc)_2{\cdot}H_2O]$ in THF, i.e. in a solvent in which assembly does not occur, and secondly by mixing the **BTA P** copper complex and one of the BTA Cha enantiomer in toluene (after THF evaporation). Transparent solutions were obtained at 293 K after brief heating of the mixtures up to boiling point, except for copper-rich mixtures (BTA P/[Cu] = 1) for which some residual non-coordinated copper can be observed (see discussion below). However, all investigated solutions exhibit similar absorbances (Figures 1 and S1) thus indicating that no significant precipitation occurs. CD and UV-Vis analyses of copper-free S&S-type mixtures are shown in Figure 1a together with those previously recorded for copper-containing mixtures.[47] All mixtures contain the same quantity of **BTA P** (5.8 mM), a concentration that ensures the formation of long hydrogen-bonded helical stacks.[60] The fraction of **BTA (*S*)-Cha** introduced in the sample, denoted as fs^0, was varied between 0.1% and 52%. All mixtures exhibit a similar CD band in the region for which only **BTA P** absorbs, i.e. the region where the signal is due to the phosphine moiety of **BTA P** induced by the "sergeant" within the helical coassemblies. A minor shift of this induced CD (ICD)[62] band is seen between copper-free ($\lambda_{max} \approx 310$ nm) and copper-containing mixtures ($\lambda_{max} \approx 290$ nm) indicating a modest modification of the π-π^* and n-π^* electronic transitions of the phosphine ligand upon coordination to [Cu]. A more drastic difference is observed for the evolution of the intensity of the ICD band as a function of fs^0. The intensity of the ICD band is indeed significantly higher for the copper-free mixtures containing less than 20% of **BTA (*S*)-Cha**. The most obvious difference is seen for the solutions containing ca. 10% of "sergeants", where the ICD reaches 75% versus 54% of its maximal value for copper-free and copper-containing mixtures, respectively (Figure 1b). On the contrary, the fact that similar intensities are reached at high fs^0 values indicates that homochiral helices are formed for "sergeant"-rich solutions whether copper is present or not.

These CD analyses were repeated several times: very small standard deviations were noticed for copper-free solutions whilst higher standard deviations were found for copper-containing mixtures, notably for $fs^0 \leq 20\%$ (Figures 1c, S1, and S2). This can be ascribed to slightly different levels of aggregation between the supramolecular helices present in these "sergeant"-poor mixtures (see below). Kuhn anisotropic values (g values) are extracted for all compositions and are plotted against fs^0 for mixtures without copper and with copper for different **BTA P**/[Cu] ratios (Figure 1c). On the one hand, this plot unambiguously confirms the significant differences in

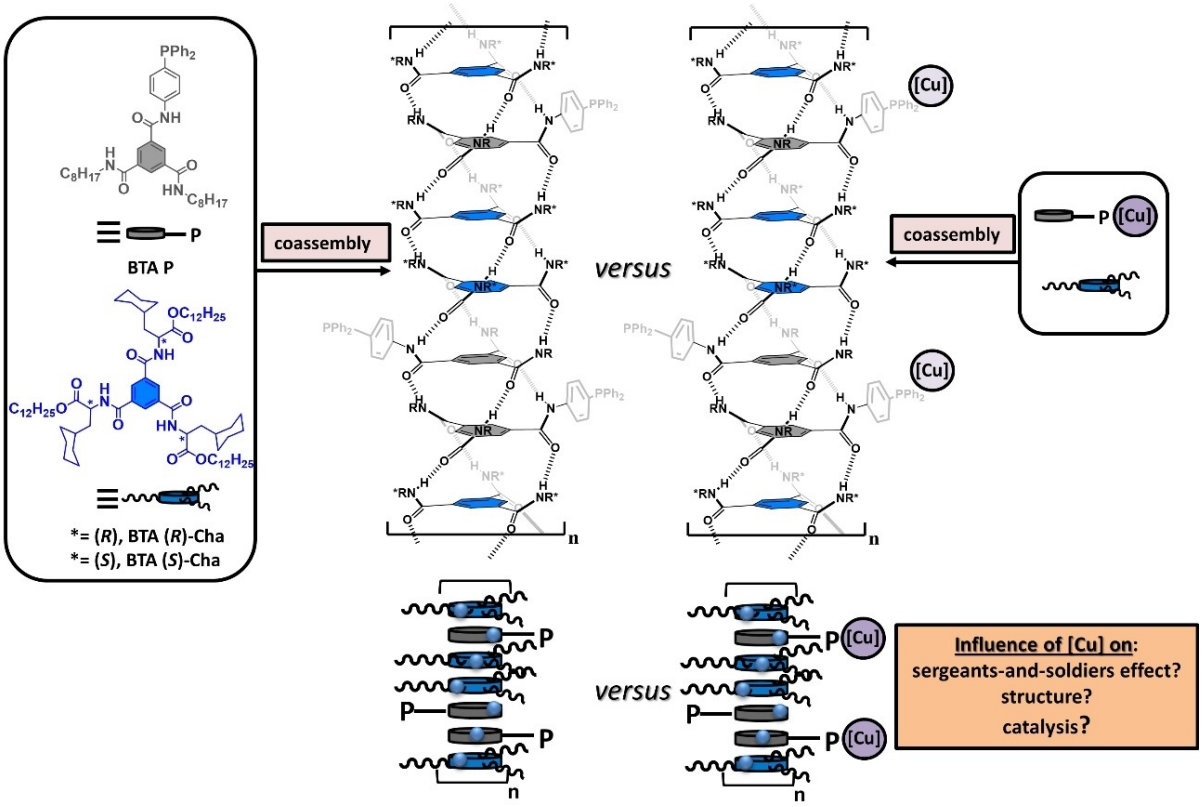

Scheme 1. Molecular structures of the BTA monomers used in this study and representation of the S&S-type assemblies formed with and without [Cu] coordinated to the phosphine groups. [Cu] represents Cu(II) and Cu(I) complexes formed upon reacting BTA P and $[Cu(OAc)_2{\cdot}H_2O]$ (see the characterization part for more information). Only "sergeant"-rich S&S assemblies are represented; for other stoichiometries see the text and Figure 5.

optical purity of the helices in the low-"sergeant" regime (compare the black and blue curves). On the other hand, the ratio of copper does not significantly alter the chiroptical properties of the copper-bound helices in the present system (blue curves).

Correlation between chiroptical and catalytic properties

In order to correlate the catalytic properties of the S&S-type helices with their chiroptical properties, the aforementioned copper-containing mixtures were engaged in the hydrosilylation of 4-nitroacetophenone (NPnone). It is worth noting here that copper-hydride active species are formed in situ upon addition of phenylsilane, which both promotes the catalytic reaction and acts as a stoichiometric reductant.[63,64] The optical purity of the catalytic product, NPnol, was determined by chiral GC analyses; **BTA (*R*)-Cha** provides (*S*)-NPnol as the major enantiomer whilst **BTA (*S*)-Cha** yields (*R*)-NPnol (see Tables S2–S4). Catalytic experiments for mixtures with **BTA P**/[Cu] = 4 were made in triplicate (Figure S2). Repeatability was excellent except for the mixtures with ca. 20% of "sergeant", likely because of the aforementioned aggregation process between helices in this regime.

The ratio of [Cu] versus **BTA P** was subsequently varied while adapting the amount of NPnone to maintain the catalytic loading in $[Cu(OAc)_2{\cdot}H_2O]$ equal to 3 mol% (Figure 2a). Overall, no dramatic influence of the **BTA P**/[Cu] ratio on the selectivity of the reaction is observed. However, lower BTA P/[Cu] ratios appear to provide slightly higher enantioselectivities, notably for mixtures with intermediate fs^0 values. The origin of this slight variation of the selectivity as function of the ratio of [Cu] does not seem to be directly related to a difference in the chiroptical properties of the copper-bound helices (Figure 1c).[65]

More importantly, enantioselectivities in NPnol, as determined from catalytic experiments shown in Figure 2a, were tentatively correlated to the g values reported in Figure 1c. The objective here is to check whether the selectivity of the catalytic reaction (*e.e.* in NPnol) is proportional to the optical purity of the copper-free and copper-bound helices (g values extracted from the CD and UV-Vis spectra). On the one hand, it appears very clearly that *e.e.* values (obtained from copper-based catalysts) and g values determined for mixtures without [Cu] follow quite different progressions as a function of fs^0. The plot of the *e.e.* values as a function of g values obtained for copper-free mixtures confirms this point since no correlation is found between these two variables (Figure 2b). This is due to the fact that the measured *e.e.* values are significantly lower than those expected upon considering the optical purity of the copper-free helices. On the other hand, a linear relationship is obtained if enantioselectivities are plotted against the optical purities of

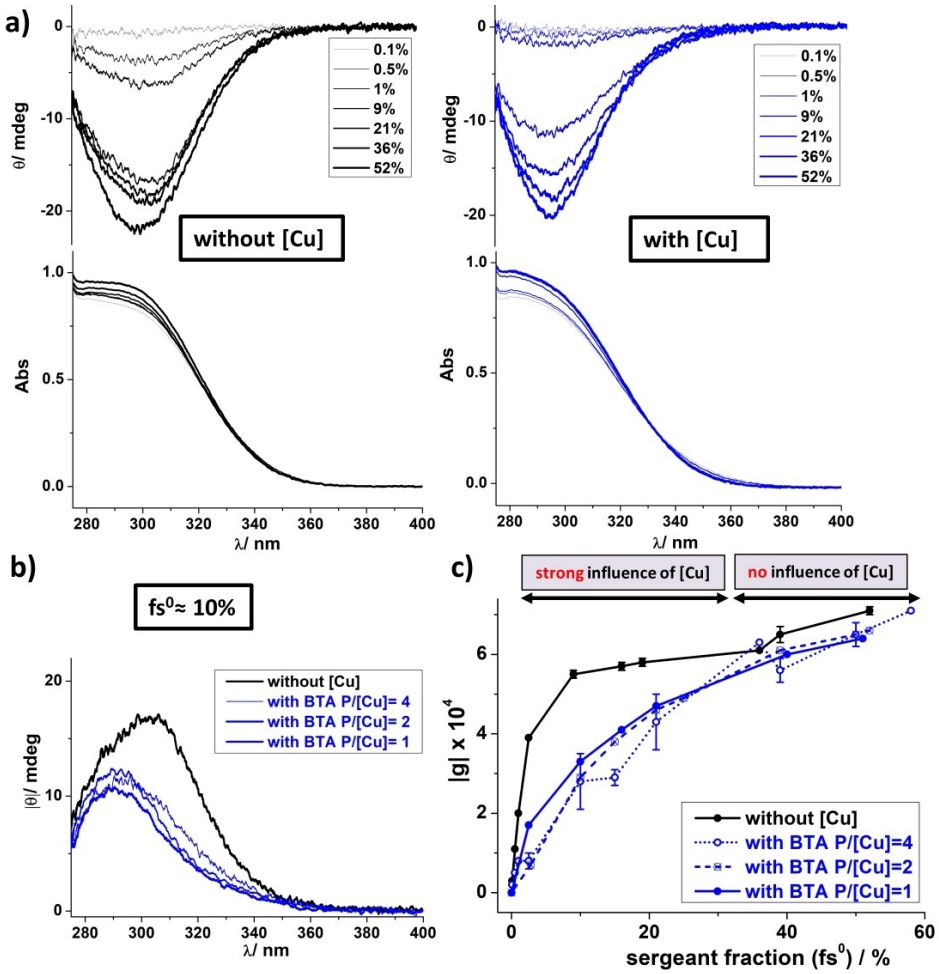

Figure 1. Chiroptical properties of the S&S-type mixtures with and without [Cu] (C_7H_8, 293 K). a) CD and UV-Vis analyses of S&S-type mixtures containing BTA P (5.8 mM), BTA (*S*)-Cha (0.06–6.35 mM, $0.1\% \leq fs^0 \leq 52\%$) with and without $[Cu(OAc)_2{\cdot}H_2O]$ (1.45 mM, BTA P/$[Cu(OAc)_2{\cdot}H_2O] = 4$). In the case of the copper-free solutions, the variation of the UV-Vis intensity is ascribed to small variations in the concentration of BTA P and/or in the cell pathlength. In the case of the copper-containing solutions, whilst contribution of the precedent reasons cannot be discarded, variation in the UV-Vis intensity is mainly related to the transition between single and crosslinked helices (see rationalization of the effect of [Cu]). b) Comparison of the CD analyses (in absolute value of ellipticity) for S&S-type mixtures containing ca. 10% of BTA (*S*)-Cha. Mixture without [Cu]: $fs^0 = 9\%$; mixture with BTA P/[Cu] = 4: $fs^0 = 9\%$; mixture with BTA P/[Cu] = 2: $fs^0 = 15\%$; mixture with BTA P/[Cu] = 1: $fs^0 = 10\%$. c) Plot of the g values recorded at $\lambda = 295$ nm as a function of fs^0 for mixtures with and without [Cu]. Kuhn anisotropy factor (g), is defined as $g = \theta/(32980 \times Abs)$ where θ and Abs are the ellipticity and UV/Vis absorbance measured at $\lambda = 295$ nm, from the CD and UV-Vis spectra respectively. Error bars for g values correspond to one standard deviation (determined from repeated measurements, see the Supporting Information).

copper-bound helices (Figure 2c). This agrees well with the previously-observed correlation between *e.e.* (up to optimal selectivity) and g values of copper-containing S&S-type mixtures, demonstrated for different "sergeants".[60] The correlation plots presented in Figure 2b and Figure 2c: i) support the significant difference between the chiroptical properties of copper-bound and copper-free helices, and ii) indicate that optical purities of the copper acetate complexes are similar to that of copper catalytic species generated during the catalytic experiments, allowing a good correlation between the *e.e.* and g values as long as the latter are recorded for copper-bound helices.

Probing the effect of copper on the structure of the S&S-type assemblies

In order to rationalize the different chiroptical properties of copper-free and copper-bound assemblies, the corresponding helices were characterized by various analytical techniques. S&S-type mixtures with $fs^0 = 9\%$ and $fs^0 = 39\%$ were selected given that the corresponding helices for $fs^0 = 9\%$ are markedly affected by the presence of copper whilst those with $fs^0 = 39\%$ exhibit similar behavior. A first hint comes from the macroscopic observation of these solutions. The solution with copper and $fs^0 = 9\%$ becomes turbid and viscous upon standing for 1 day whilst all others mixtures remain clear and fluid (Figure S3a and movies 1). The increase in viscosity is observed only for the solution with **BTA P**/[Cu] = 4, not for the other

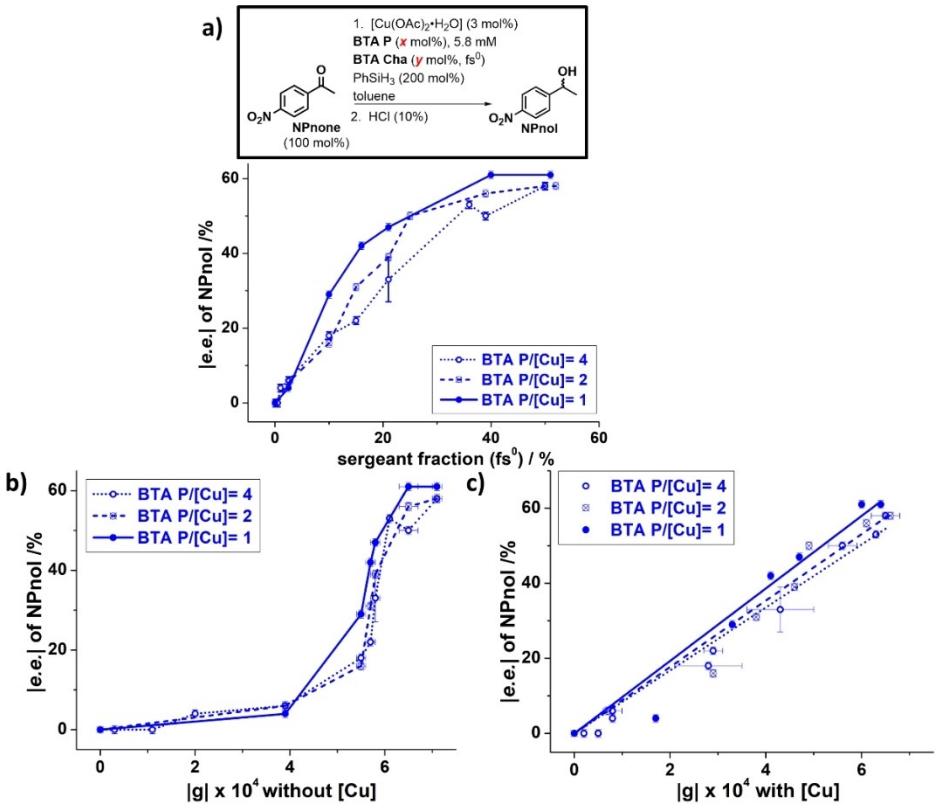

Figure 2. Correlation between chiroptical and catalytic properties (C_7H_8, 293 K). a) Plot of the enantioselectivity (*e.e.*) in NPnol versus the fraction of BTA Cha (fs^0) in the mixtures. Conditions for the catalytic reactions: BTA P (5.8 mM, 3, 6 or 12 mol%), $[Cu(OAc)_2{\cdot}H_2O]$ (3 mol%), BTA Cha (0.006–6.35 mM), NPnone (48, 96 or 192 mM, 100 mol%), $PhSiH_3$ (200 mol%), 293 K. Conversion > 99% was obtained for all catalytic experiments, as determined by GC and ^{1}H NMR analyses. The optical purity was determined by chiral GC analyses. Standard deviations of *e.e.* for repeated experiments with BTA P/[Cu] = 4 are lower than the uncertainty for *e.e.* measurement (±1%, HPLC analysis) except for $fs^0 = 21\%$ (±6%). b) Plot of the enantioselectivity in NPnol versus g values without [Cu]. Enantiomeric excesses correspond to values plotted in Figure 2a whilst g values are those extracted for the CD and UV-Vis spectra of copper-free mixtures and plotted in Figure 1c (black curve). These values are compiled in Table S4. c) Plot of the enantioselectivity in NPnol versus g values with [Cu]. Enantiomeric excesses correspond to values plotted in Figure 2a whilst g values are those extracted for the CD and UV-Vis spectra of copper-containing mixtures and plotted in Figure 1c (blue curves corresponding to the different BTA P/[Cu] ratios). These values are compiled in Table S4. Linear fitting is performed with a zero-intercept fixed at origin. It yields the following values: slope of 9.7 ± 0.5% *e.e.*/g unit and $R^2 = 0.98$ for BTA P/[Cu] = 1, slope of 8.8 ± 0.3% *e.e.*/g unit and $R^2 = 0.99$ for BTA P/[Cu] = 2, slope of 8.4 ± 0.3% *e.e.*/g unit and $R^2 = 0.99$ for BTA P/[Cu] = 4.

stoichiometries corresponding to copper-enriched helices (Figure S3b and movies 2). Aggregation between BTA helices, promoted by copper atoms acting as crosslinks, are likely responsible for this rheological behavior. The copper-rich mixture with **BTA P**/[Cu] = 1, shows some insoluble blue solids that can be ascribed to non-coordinated copper, with no specific band detected in the visible region (Figure S4).

It is worth noting here that the aggregation process towards highly crosslinked helices seems relatively slow (on the timescale of tens of hours), but aggregation is already present after dissolution as demonstrated by the aforementioned analyses. The increase in viscosity for the solution with **BTA P**/[Cu] = 4, is accompanied by a modest decrease of the g value, indicating that most of the chiral defects are already present a few minutes after dissolution (Figure S5).[66,67]

SANS analyses performed a few hours after dissolution indicate that all solutions contain mostly cylindrical objects as indicated by the q^{-1} dependency of the scattered intensity (Figure 3a). However, a major difference is seen for the solutions with $fs^0 = 9\%$ and [Cu] that clearly exhibit a deviation from the q^{-1} slope at moderate and low q values. This roughly q^{-3} dependency of the scattered intensity can be attributed to the formation of large aggregates, i.e. crosslinked cylinders. Increasing the amount of [Cu] leads to objects exhibiting a higher scattered intensity in the same region (Figure 3b) but the exact amount and nature of aggregates in these solutions cannot be determined precisely. Importantly, these aggregates are not significant for the same solution containing a higher fraction of **BTA (*S*)-Cha** ($fs^0 = 39\%$). SANS curves for the solutions with $fs^0 = 39\%$ are fitted considering a mixture of cylindrical objects, for **BTA P** (or **BTA P**·[Cu]) and **BTA (*S*)-Cha** helical co-assemblies, and spherical objects, for **BTA (*S*)-Cha** dimers.[68–73] Good fits are obtained by assuming a radius for the cylinders (11 ± 1 Å) that is consistent with a single BTA molecule in the cross-section, i.e. single helices (see the experimental section for more details and Figure S6 for the SANS curves of the individual components).[60] The fraction of **BTA (*S*)-Cha** that is actually present in the stacks, fs^s, can also be extracted from these fits: $fs^s = 36\%$ and 25% for helical co-assemblies with and without [Cu], respectively. The former value agrees well with that

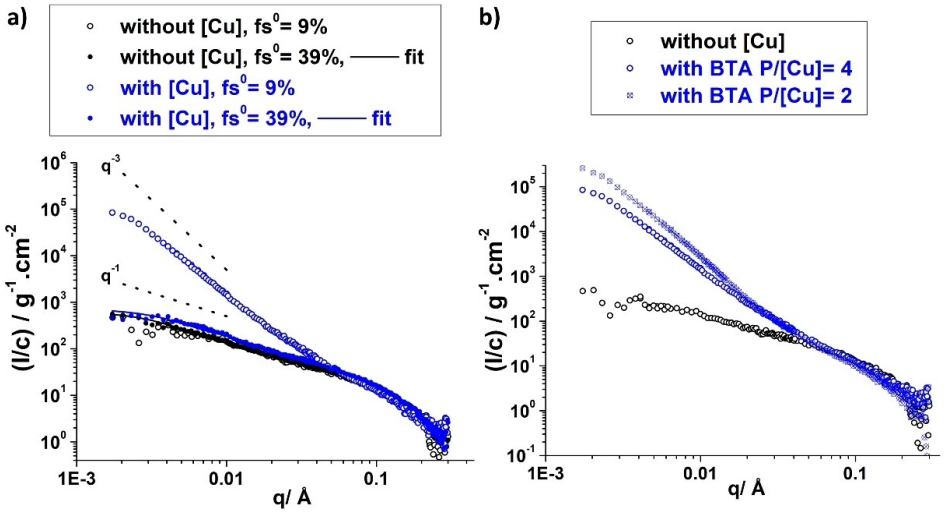

Figure 3. SANS analyses of S&S-type mixtures with and without [Cu] (C_7D_8, 293 K). a) Scattered intensity (cm^{-1}) normalized by the total BTA concentration for the S&S-type mixtures containing BTA P (4.0 $g.L^{-1}$, 5.8 mM) and BTA (*S*)-Cha (0.68 $g.L^{-1}$, 0.58 mM, $fs^0 = 9\%$ or 4.4 $g.L^{-1}$, 3.8 mM, $fs^0 = 39\%$) with and without $[Cu(OAc)_2{\cdot}H_2O]$ (0.29 $g.L^{-1}$, 1.45 mM, BTA P/[Cu] = 4) in C_7D_8. The SANS curves for $fs^0 = 39\%$ were fitted considering a mixture of cylinders and spheres (see the experimental section for more details). b) Scattered intensity (cm^{-1}) normalized by the total BTA concentration for the S&S-type mixtures containing BTA P (4.0 $g.L^{-1}$, 5.8 mM) and BTA (*S*)-Cha (0.68 $g.L^{-1}$, 0.58 mM, $fs^0 = 9\%$) with various ratios of $[Cu(OAc)_2{\cdot}H_2O]$ (0.29 $g.L^{-1}$, 1.45 mM for BTA P/[Cu] = 4; 0.58 $g.L^{-1}$, 2.90 mM for BTA P/[Cu] = 2) in C_7D_8.

reported for an identical mixture but analyzed during a former SANS beamtime ($fs^s = 29\%$).[60]

The composition of the BTA helices can also be deduced from FTIR analyses since helical co-assemblies and BTA Cha dimers have drastically different signatures (Figure S7).[58–61] It also allows to get the fs^s values for solutions that contain aggregated helices and for which SANS analyses cannot be fitted precisely. Satisfactory fits of the FTIR curves in the N–H and C=O regions (Figure S8), provide the fractions of "sergeant" in stacks compiled in Table 1. The fs^s values for the $fs^0 = 39\%$ solutions deduced from FTIR and SANS analyses are in fair agreement (Table 1) considering that precision of the SANS fits is sensitive to small fluctuations in the scattered intensity. In addition, SANS and FTIR data show the same trend: BTA Cha molecules are incorporated more efficiently into the copper-bound helices versus copper-free helices. This seems to be true for both single helices ($fs^0 = 39\%$) and crosslinked helices ($fs^0 = 9\%$). One possible reason is that copper-bound helices are longer than copper-free ones, because of the decrease of the hydrogen bond acceptor capability of the phosphine moieties upon coordination to copper.[59] Better incorporation of BTA Cha molecules would thus be driven by a more favorable entropy of mixing. The slightly higher fraction of BTA Cha into the stacks of copper-bound helices should have led to higher optical purity for the corresponding helical co-assemblies, given the propensity of BTA Cha to remove chiral defects upon intercalation.[60] This is actually opposite to what it observed for CD analyses of the solutions with $fs^0 = 9\%$ (Figure 1) and therefore, the different chiroptical properties between copper-bound and copper-free helices cannot be explained by this slightly difference in the composition of the co-assemblies.

We looked whether the presence of crosslinked helices, in addition to the lowered CD intensities detected in Figure 1, led to specific spectroscopic signatures compared to single helices. FTIR analyses of crosslinked and single helices do not reveal any remarkable difference indicating that the hydrogen-bond network is similar for the two types of helices (Figure S7). Closer examination of the aforementioned CD and UV-Vis analyses reveal minor differences. Normalized CD and UV-Vis data for copper-free solutions show no significant change in the shape of CD and UV-Vis bands when going from poorly helically-biased helices, for low and intermediate fs^0 values, to homochiral helices, for high fs^0 values (Figure S9a). This is consistent with the presence of only one type of co-assemblies, namely single helices (as deduced from SANS in Figure 3). However, the same analyses for copper-containing S&S-type mixtures, exhibit a narrowing of the main CD band upon increasing the fraction of "sergeants" in the mixtures (Figure S9b). In addition, a gradual increase of the intensity of the main UV-Vis band is seen for the same mixtures (Figure 1a). This slight changes in the shape and intensity of the CD and UV-Vis bands can be explained by a modification of the conformation of the PPh_2

Table 1. Geometrical features and composition of the S&S-type co-assemblies determined from SANS and FTIR data (**BTA P**/[Cu] = 4).

S&S-type mixtures	fs^s [%] from SANS	fs^s [%] from FTIR	Geometry[a]
$fs^0 = 9\%$ without [Cu]	nd	4.5	single helices
$fs^0 = 9\%$ with [Cu]	nd	6	crosslinked helices
$fs^0 = 39\%$ without [Cu]	25	17	single helices
$fs^0 = 39\%$ with [Cu]	36	28	single helices

unit when going from crosslinked to single helices (see the discussion below).

We finally probe whether additional information can be extracted from the $^{31}P\{^1H\}$ NMR traces of the copper-free and copper-containing mixtures (see Figures S10 and S11 for additional NMR spectra and for a more detailed interpretation). On the one hand, a single signal is present ($\delta = -5.2$ ppm) that accounts for the free phosphine moiety in helical co-assemblies without [Cu] (Figure 4). In the other hand, copper complexes for the two selected S&S compositions exhibit drastically different ^{31}P NMR traces. Crosslinked helices, present in the sample embedding 9% of **BTA (*S*)-Cha**, show a broad asymmetric signal ($\delta_{max} \approx -3$ ppm) whilst single helices, present in the sample containing 39% of **BTA (*S*)-Cha**, exhibit two broad but distinguishable signals at $\delta = -1.8$ ppm and $\delta = -5.2$ ppm. The latter and former signals are attributed to **BTA P**·[Cu] and free **BTA P**, respectively.

These data suggest that the exchange rate of [Cu] between free and copper-bound phosphines is affected by the aggregation ability of the BTA monomers. It is reasonable to envisage that in the copper crosslinked helices with a small fraction of "sergeants", **BTA P** sites are sufficiently close to exchange their copper atoms, and consequently close to coalescence (or large broadening) of the ^{31}P signals is observed under these conditions. Finally, exchange rate of copper atoms between **BTA P** and **BTA P**·[Cu] centers is expected to be rather slow in single helices as these groups are separated by a larger fraction of "sergeants". These NMR analyses do not allow to determine a precise structure for the **BTA P**·[Cu] complexes but indicate differences in the exchange rates between **BTA P** and **BTA P**·[Cu] sites that can be reasonably explained by the structure and composition of helical co-assemblies, as deduced from the aforementioned FTIR and SANS analyses.

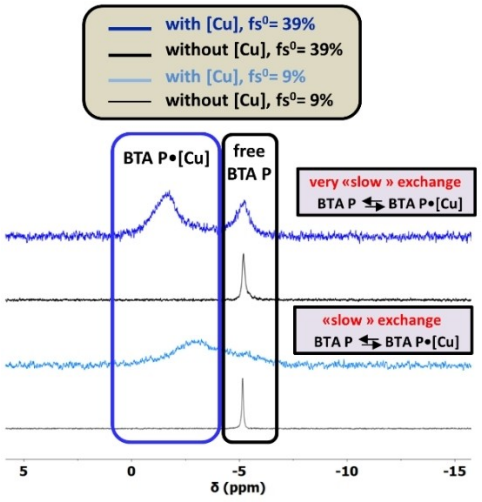

Figure 4. $^{31}P\{^1H\}$ NMR analyses of S&S-type mixtures with and without [Cu] in C_7D_8 at 293 K. NMR analyses of the S&S-type mixtures containing BTA P (5.8 mM) and BTA (*S*)-Cha (0.58 mM, $fs^0 = 9\%$; or 3.8 mM, $fs^0 = 39\%$) with and without $[Cu(OAc)_2{\cdot}H_2O]$ (1.45 mM, BTA P/[Cu] = 4). Full $^{31}P\{^1H\}$ NMR spectra showing the presence of BTA P=O and potentially BTA P=O·[Cu] species are shown in Figure S11.

Proposed rationale for the different properties between copper-free and copper-bound S&S-type helices

Analytical data reveal a significant effect of copper-binding on the chiroptical and structural properties of S&S-type helical co-assemblies composed of **BTA P** and BTA Cha. Two main regimes are observed ([I] and [II], Figure 5). At high fraction of BTA Cha ([II]), the presence of copper does not significantly alter the nature of the assemblies: the only notable difference is a slightly better incorporation of BTA Cha into the stacks when copper is present at the periphery of the helices. Homochiral single helices are observed with and without [Cu] and the selectivity of the reaction is optimal. At low fraction of BTA Cha ($fs^0 \leq 20\%$, regime [I]), the most striking structural difference is the presence of copper crosslinked helices that exhibit lower optical purities than copper-free single helices. The selectivity of the hydrosilylation reaction correlates only with the optical purity of copper-bound assemblies thus indicating that the rearrangement induced by copper centers must be considered to rationalize the extent of enantioselectivity in S&S-type helical BTA catalysts.

From the presented data, it can be surmised that the copper crosslinks consist of copper atom(s) connected to two or more **BTA P** monomers belonging to different helices as represented in Figure 5. Dimeric $[Cu_2(OAc)_4]$ species with phosphine moieties occupying the axial positions can be discarded given the absence of its characteristic signature in the visible region (Figure S4).[74,75] BTA Cha, even though it does not interfere directly with the copper complex, modulates the coordination sphere around the copper probably because it provides some bulkiness in proximity of the BTA P·[Cu] monomers that prevents the ligation of phosphine moieties by different helices in regime [II] (see the dotted arrows in Figure 5). It is indeed reasonable to consider that the side chains of BTA Cha, i.e. the dodecyl ester of cyclohexylalanine, would generate more steric hindrance than the octyl and PPh_2 groups of **BTA P** that mostly surround the [Cu] centers in regime [I]. The good correlation between the selectivity outcome and the optical purity of the helices suggests that the multi-ligated copper centers in crosslinked helices do not directly lower the selectivity by themselves but rather that these crosslinks induce chiral defects, probably because structural constraints for copper coordination are not compatible with the optimal stacking of BTA monomers in the helical co-assemblies.

The maximal number of crosslinks in the present system seems to be reached when the **BTA P** to $[Cu(OAc)_2{\cdot}H_2O]$ ratio is equal to 4 since a gel is formed only for that ratio (Figure S3 and movies). Whilst a value of two **BTA P** by $[Cu(OAc)_2{\cdot}H_2O]$ could have been expected to yield a maximal number of crosslinks, the experimentally-determined ratio can be explained by the partial oxidation of **BTA P** concomitantly to the generation of [Cu] complex, that decreases the actual number of free phosphine available for copper coordination. Phosphine oxides have lower ability than phosphines for coordinating relatively soft copper atoms and are thus probably not involved as ligands for the copper crosslinks.

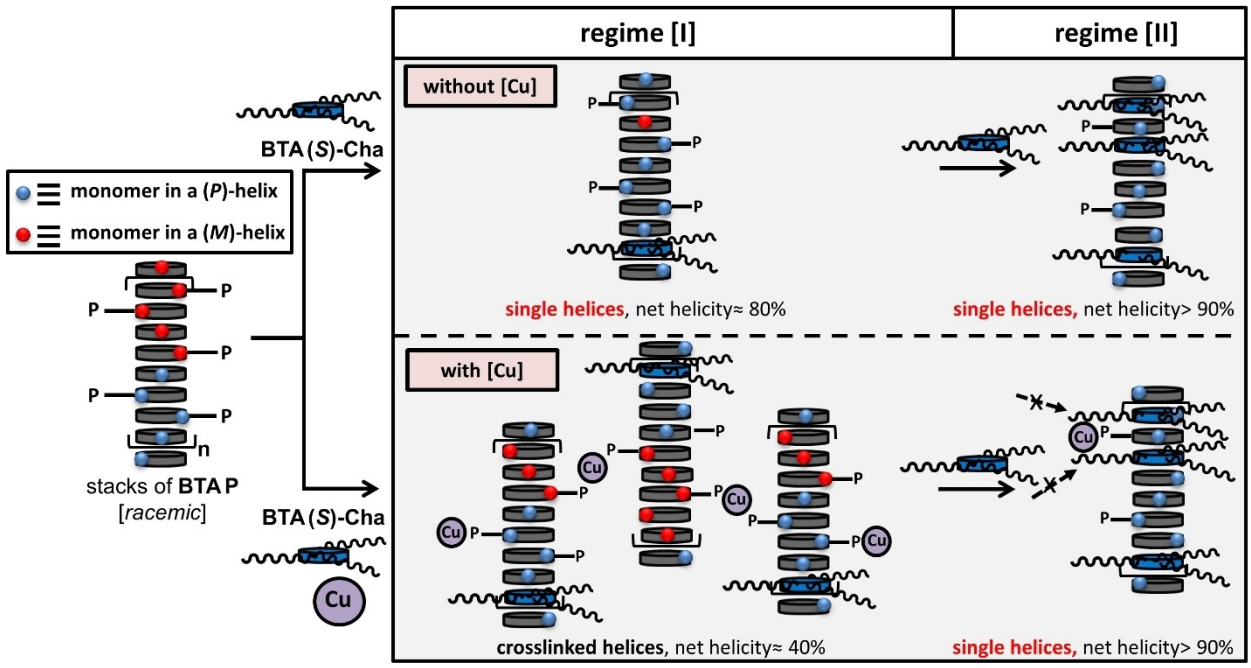

Figure 5. Schematic representation of the effect of copper crosslinks on the structure and chiroptical properties of S&S-type assemblies between BTA P and BTA (*S*)-Cha. BTA (*S*)-Cha favors the formation of (*P*)-helices as represented. BTA P=O and potentially BTA P=O·[Cu] species detected by ^{31}P NMR are not represented. Dotted arrows in the regime [II] with [Cu] indicate that the side chains of BTA (*S*)-Cha (i.e. the dodecyl ester of cyclohexylalanine) generate steric hindrance around the [Cu] center which prevents coordination of a PPh_2 moiety belonging to another helix, hence the crosslinking of supramolecular helices.

It is not clear whether the slightly higher enantioselectivities observed for copper-rich helices is related to their lower number of crosslinks since no clear differences in the optical purities of the helices have been detected for the different ligand to copper stoichiometries. This marginal discrepancy can be explained either by a structural difference between copper acetate complexes (characterized by CD) and copper hydride species (active in catalysis) or by the presence of different copper-active complexes for the different **BTA P**/[Cu] ratios.

In their seminal studies, Green and co-workers observed a sharp increase in the optical purity of the helical poly(n-hexyl isocyanate) incorporating 0.5% of (*R*)-2,6-dimethylheptyl isocyanate upon lowering the temperature in hydrocarbon solvents.[14] This sudden change occurs concomitantly to the formation of gels and it was thus surmised that physical crosslinks reduces the number of helix reversals.[15] In supramolecular polymers of disc-like molecules, helical bundles formed upon interdigitation of the peripheral helical groups have been found to be responsible for a spontaneous mirror-symmetry breaking phenomenon leading to helically-biased stacks from achiral monomers,[76–79] or to heterochiral bundles selectively formed upon social self-sorting of racemic helices.[51] Our work indicates that crosslinks between supramolecular chains can also lower the optical activity of supramolecular helices and hence aggregation must be considered as an important parameter for the modulation of the chiroptical properties of BTA and related assemblies of disc-like molecules.

Conclusion

The extent of the "sergeant-and-soldier" effect in supramolecular BTA helices composed of a catalytically-active ligand and an enantiopure BTA monomer is decreased upon coordination of the phosphine moieties of the ligand to $[Cu(OAc)_2{\cdot}H_2O]$. Data supports that copper crosslinks, generated upon coordination of phosphine moieties belonging to different helices, are responsible for the diminished optical purity of the BTA helices. These crosslinks are dynamic by essence and are found to be eliminated when a sufficient amount of "sergeant" is present in the helices. Our work demonstrates that copper or other metal binding groups can be envisaged to introduce dynamic crosslinks in supramolecular materials, thus constituting an alternative strategy to difunctionalized linkers reported to date.[80–82] Not only main chain but also side chain aggregation of supramolecular helices must be considered for the design of elaborated chiral materials. Improving the extent of the "sergeants-and-soldiers" effect in catalytic BTAs by tuning the aggregation of the supramolecular chains is currently under investigation in our laboratory.

Experimental Section

Materials: BTA P,[58] and BTA Cha enantiomers[69] were synthesized as reported previously. **BTA (*S*)-Cha** and **BTA (*R*)-Cha** used in this study were purified by preparative HPLC as reported leading to optically-pure samples.[60] 1-(4-nitrophenyl)ethanone (>98%, Alfa Aesar), $PhSiH_3$ (>97%, Alfa Aesar) and $[Cu(OAc)_2{\cdot}H_2O]$ (>99%, Alfa

Aesar) were used as received. Dried THF and toluene were obtained from a Solvent Purification System (SPS). THF-d_8 and C_7D_8 were bought from Eurisotop and used without further purification. Only freshly opened bottles of THF-d_8 were used in order to avoid the presence of peroxides.

Methods: Fourier-Transform Infrared (FTIR) analyses: FTIR measurements were performed on a Nicolet iS10 spectrometer. Spectra of solutions in toluene were measured in 0.05 cm pathlength CaF_2 cells at 293 K and were corrected for air, C_7D_8 and cell absorption (Figures S7 and S8). Procedure for simulated FTIR spectra (see Figure S8 for the results): S&S-type mixtures containing **BTA P** (5.8 mM), **BTA (*S*)-Cha** (0.58 mM, $fs^0 = 9\%$) with and without $[Cu(OAc)_2{\cdot}H_2O]$ (1.45 mM):[60] The influence of the stack ends is neglected. Here, the concentration of dimers cannot be extracted by fitting the ester carbonyl region of the experimental FTIR spectrum (1700–1800 cm^{-1}) because the amount of **BTA (*S*)-Cha** is too small. Simulated spectra (Figure S8) are built by presuming a fraction of **BTA (*S*)-Cha** as dimers and adding the FTIR spectra of these dimers, of **BTA P** (5.8 mM) or **BTA P**·[Cu] (**BTA P** 5.8 mM + $[Cu(OAc)_2{\cdot}H_2O]$ 1.45 mM), and of **BTA Met**[68] (at the concentration of the "sergeant" in stacks). The simulated spectra that fit best the experimental ones yield a plausible value for the fraction of **BTA (*S*)-Cha** in stacks (fs^s from FTIR in Table 1). S&S-type mixtures containing **BTA P** (5.8 mM), **BTA (*S*)-Cha** (3.8 mM, $fs^0 = 39\%$) with and without $[Cu(OAc)_2{\cdot}H_2O]$ (1.45 mM):[60] As no free N–H can be detected in the FTIR spectra of these mixtures, the influence of the stack ends is neglected. The concentration of dimers is extracted by fitting the ester carbonyl region of the experimental FTIR spectrum (1700–1800 cm^{-1}) with the individual spectra of **BTA (*S*)-Cha** (representative of dimers, bonded ester C=O, $\nu \approx 1725\ cm^{-1}$) and of **BTA Met**[68] (reference for "sergeants" in stacks, free ester C=O, $\nu \approx 1745\ cm^{-1}$). The fraction of **BTA (*S*)-Cha** in stacks is thus deduced from the concentration of remaining dimers (fs^s from FTIR in Table 1). The addition of the FTIR spectra of the remaining dimers, of **BTA P** (5.8 mM) or **BTA P**·[Cu] (**BTA P** 5.8 mM + $[Cu(OAc)_2{\cdot}H_2O]$ 1.45 mM), and of **BTA Met** (at the concentration of the "sergeant" in stacks) yields the simulated spectra (Figure S8). The good fit between experimental and simulated spectra validates the fs^s values.

Circular dichroism (CD) analyses: CD measurements were performed on a Jasco J-1500 spectrometer equipped with a Peltier thermostated cell holder and Xe laser. Data were recorded at 293 K with the following parameters: 50 $nm.min^{-1}$ sweep rate, 0.05 nm data pitch, 2.0 nm bandwidth, and between 400 and 275 nm. Spectra in Figure S4 were recorded up to 800 nm to discard the presence of $[Cu_2(OAc)_4]$ dimers. All solutions were pre-heated prior to measurements. Toluene and cell contributions at 293 K were subtracted from the obtained signals. Cylindrical spectrosil quartz cells of 0.10 mm pathlength (Starna® 31/Q/0.1) were used. For all samples, LD contribution was negligible ($\Delta LD < 0.005$ dOD) and the shape of the CD signal was independent of the orientation of the quartz cells.

UV-Vis analyses: UV-Vis absorption spectra were extracted from CD on each of the above samples and obtained after correction of the absorption of air, solvent, and cell at 293 K.

Small-angle neutron scattering (SANS) analyses: SANS measurements were made at the LLB (Saclay, France) on the PA20 instrument, at three distance-wavelength combinations to cover the 2×10^{-3} to 0.3 $Å^{-1}$ q-range, where the scattering vector q is defined as usual, assuming elastic scattering, as $q = (4\pi/\lambda)\sin(\theta/2)$, where θ is the angle between incident and scattered beam. Data were corrected for the empty cell signal and the solute and solvent incoherent background. A light water standard was used to normalize the scattered intensities to cm^{-1} units. The data was fitted with the DANSE software SasView. The data for the mixtures was modelled by the combination of cylinders and spheres. The cylinders are assumed to be composed of all **BTA P** (the "soldiers") and a fraction of the **BTA (*S*)-Cha** molecules (the "sergeants"). The spheres are assumed to consist in the remaining "sergeant". The only adjustable parameter was the proportion of "sergeants" that co-assemble with **BTA P** into cylinders. The radius of both cylinders and spheres was fixed (11 ± 1 Å) because this value is consistent with the radius obtained by fitting the SANS curves in C_7D_8 of the individual components of the mixtures.[59] The scattering length densities (SLD) for the spheres were calculated from the atomic bound coherent scattering lengths (value of $0.506\times10^{-6}\ Å^{-2}$ for **BTA (*S*)-Cha**).[60] The SLD for the cylinders were calculated by averaging the molecular SLD according to the composition of the cylinders. The mixtures with $fs^0 = 9\%$ were not fitted because of the uncertainty related to the aggregation (for **BTA P**·[Cu] mixture) and to the low number of introduced "sergeant" (for both **BTA P**·[Cu] and **BTA P** mixtures). The mixtures with **BTA P**/[Cu] = 2 were not fitted because of aggregation.

NMR analyses: NMR spectra were recorded on a Bruker Avance 400 spectrometer or JEOL ECZ400S/L1 operating at a ^1H Larmor frequency of 400 MHz with a 5 mm broadband probe head $^1H/^{19}F/^{31}P-^{15}N$ (BBFO or Royal HFX probe). The ^1H NMR spectra were recorded using a pulse sequence of proton with a spectral width of 7183 Hz, an acquisition time of 4.6 s and a relaxation delay of 1 s. Calibration has been done on the residual solvent peak: THF-d_8 (^1H: 1.72 ppm), C_7D_8 (^1H: 2.08 ppm). The ^{31}P NMR spectra were recorded using a pulse sequence $^{31}P\{^1H\}$ with a spectral width of 24300 Hz, an acquisition time of 1.3 s and a relaxation delay of 2 s. A sample of H_3PO_4 85% in D_2O is used to calibrate the chemical shift reference at 0 ppm. The value of this reference is filled for each spectrum thus allowing their calibration.

Acknowledgements

The French Agence Nationale de la Recherche is acknowledged for funding the project AbsoluCat (ANR-17-CE07-0002, PhD position of AH). This work was supported by the Consejo Nacional de Ciencia y Tecnologia (CONACYT, post-doctoral fellowship of M.A.M.-A.) and the China Scholarship Council (CSC, PhD grants of Y.L. and H. K.). Jacques Jestin (LLB, Saclay) is acknowledged for assistance with SANS experiment. The GDR 3712 Chirafun is acknowledged for allowing a collaborative network.

Conflict of Interest

The authors declare no conflict of interest.

Data Availability Statement

The data that support the findings of this study are available in the supplementary material of this article.

Keywords: benzene-1,3,5-tricarboxamide · chiral defects · crosslink · "sergeants-and-soldiers" effect · supramolecular chirality · supramolecular polymers

[1] C. Girard, H. B. Kagan, *Angew. Chem. Int. Ed.* **1998**, *37*, 2922–2959; *Angew. Chem.* **1998**, *110*, 3088–3127.
[2] L. C. Mayer, S. Heitsch, O. Trapp, *Acc. Chem. Res.* **2022**, *55*, 3345–3361.
[3] K. Soai, T. Kawasaki, A. Matsumoto, *Acc. Chem. Res.* **2014**, *47*, 3643–3654.
[4] J. Merad, P. Borkar, F. Caijo, J.-M. Pons, J.-L. Parrain, O. Chuzel, C. Bressy, *Angew. Chem. Int. Ed.* **2017**, *56*, 16052–16056; *Angew. Chem.* **2017**, *129*, 16268–16272.
[5] T. Buhse, J.-M. Cruz, M. E. Noble-Terán, D. Hochberg, J. M. Ribó, J. Crusats, J.-C. Micheau, *Chem. Rev.* **2021**, *121*, 2147–2229.
[6] Q. Sallembien, L. Bouteiller, J. Crassous, M. Raynal, *Chem. Soc. Rev.* **2022**, *51*, 3436–3476.
[7] E. Yashima, N. Ousaka, D. Taura, K. Shimomura, T. Ikai, K. Maeda, *Chem. Rev.* **2016**, *116*, 13752–13990.
[8] Y. Okamoto, T. Nakano, *Chem. Rev.* **1994**, *94*, 349–372.
[9] G. A. Metselaar, J. J. L. M. Cornelissen, A. E. Rowan, R. J. M. Nolte, *Angew. Chem. Int. Ed.* **2005**, *44*, 1990–1993; *Angew. Chem.* **2005**, *117*, 2026–2029.
[10] E. Yashima, K. Maeda, H. Iida, Y. Furusho, K. Nagai, *Chem. Rev.* **2009**, *109*, 6102–6211.
[11] M. M. Green, J.-W. Park, T. Sato, A. Teramoto, S. Lifson, R. L. B. Selinger, J. V. Selinger, *Angew. Chem. Int. Ed.* **1999**, *38*, 3138–3154; *Angew. Chem.* **1999**, *111*, 3328–3345.
[12] C. Carlini, F. Ciardelli, P. Pino, *Makromol. Chem.* **1968**, *119*, 244–248.
[13] F. Ciardelli, P. Salvadori, *Pure Appl. Chem.* **1985**, *57*, 931–940.
[14] H. Gu, Y. Nakamura, T. Sato, A. Teramoto, M. M. Green, S. K. Jha, C. Andreola, M. P. Reidy, *Macromolecules* **1998**, *31*, 6362–6368.
[15] M. M. Green, C. A. Khatri, M. P. Reidy, K. Levon, *Macromolecules* **1993**, *26*, 4723–4725.
[16] M. Liu, L. Zhang, T. Wang, *Chem. Rev.* **2015**, *115*, 7304–7397.
[17] Y. Wang, X. Li, F. Li, W.-Y. Sun, C. Zhu, Y. Cheng, *Chem. Commun.* **2017**, *53*, 7505–7508.
[18] D. Yang, P. Duan, L. Zhang, M. Liu, *Nat. Commun.* **2017**, *8*, 15727.
[19] L. Ji, Y. Sang, G. Ouyang, D. Yang, P. Duan, Y. Jiang, M. Liu, *Angew. Chem. Int. Ed.* **2019**, *58*, 844–848; *Angew. Chem.* **2019**, *131*, 854–858.
[20] P. Li, B. Lü, D. Han, P. Duan, M. Liu, M. Yin, *Chem. Commun.* **2019**, *55*, 2194–2197.
[21] A. Mukherjee, S. Ghosh, *Chem. Eur. J.* **2020**, *26*, 12874–12881.
[22] Y. Nagata, M. Uno, M. Suginome, *Angew. Chem. Int. Ed.* **2016**, *55*, 7126–7130; *Angew. Chem.* **2016**, *128*, 7242–7246.
[23] W. Mtangi, F. Tassinari, K. Vankayala, A. Vargas Jentzsch, B. Adelizzi, A. R. A. Palmans, C. Fontanesi, E. W. Meijer, R. Naaman, *J. Am. Chem. Soc.* **2017**, *139*, 2794–2798.
[24] T. Yamamoto, M. Suginome, *Angew. Chem. Int. Ed.* **2009**, *48*, 539–542; *Angew. Chem.* **2009**, *121*, 547–550.
[25] M. Suginome, T. Yamamoto, Y. Nagata, T. Yamada, Y. Akai, *Pure Appl. Chem.* **2012**, *84*, 1759–1769.
[26] Y. Li, L. Bouteiller, M. Raynal, *ChemCatChem* **2019**, *11*, 5212–5226.
[27] A. R. A. Palmans, E. W. Meijer, *Angew. Chem. Int. Ed.* **2007**, *46*, 8948–8968; *Angew. Chem.* **2007**, *119*, 9106–9126.
[28] S. Cantekin, T. F. A. de Greef, A. R. A. Palmans, *Chem. Soc. Rev.* **2012**, *41*, 6125–6137.
[29] Y. Dorca, J. Matern, G. Fernández, L. Sánchez, *Isr. J. Chem.* **2019**, *59*, 869–880.
[30] L. Brunsveld, A. P. H. J. Schenning, M. A. C. Broeren, H. M. Janssen, J. A. J. M. Vekemans, E. W. Meijer, *Chem. Lett.* **2000**, *29*, 292–293.
[31] A. J. Wilson, M. Masuda, R. P. Sijbesma, E. W. Meijer, *Angew. Chem. Int. Ed.* **2005**, *44*, 2275–2279; *Angew. Chem.* **2005**, *117*, 2315–2319.
[32] A. J. Wilson, J. van Gestel, R. P. Sijbesma, E. W. Meijer, *Chem. Commun.* **2006**, 4404–4406.
[33] M. M. J. Smulders, A. P. H. J. Schenning, E. W. Meijer, *J. Am. Chem. Soc.* **2008**, *130*, 606–611.
[34] M. M. J. Smulders, I. A. W. Filot, J. M. A. Leenders, P. van der Schoot, A. R. A. Palmans, A. P. H. J. Schenning, E. W. Meijer, *J. Am. Chem. Soc.* **2010**, *132*, 611–619.
[35] H. M. M. ten Eikelder, A. J. Markvoort, T. F. A. de Greef, P. A. J. Hilbers, *J. Phys. Chem. B* **2012**, *116*, 5291–5301.
[36] A. J. Markvoort, H. M. M. ten Eikelder, P. A. J. Hilbers, T. F. A. de Greef, E. W. Meijer, *Nat. Commun.* **2011**, *2*, 509.
[37] M. M. J. Smulders, P. J. M. Stals, T. Mes, T. F. E. Paffen, A. P. H. J. Schenning, A. R. A. Palmans, E. W. Meijer, *J. Am. Chem. Soc.* **2010**, *132*, 620–626.
[38] E. E. Greciano, J. Calbo, J. Buendía, J. Cerdá, J. Aragó, E. Ortí, L. Sánchez, *J. Am. Chem. Soc.* **2019**, *141*, 7463–7472.
[39] Y. Dorca, R. Sánchez-Naya, J. Cerdá, J. Calbo, J. Aragó, R. Gómez, E. Ortí, L. Sánchez, *Chem. Eur. J.* **2020**, *26*, 14700–14707.
[40] F. García, L. Sánchez, *J. Am. Chem. Soc.* **2012**, *134*, 734–742.
[41] T. Kim, T. Mori, T. Aida, D. Miyajima, *Chem. Sci.* **2016**, *7*, 6689–6694.
[42] M. A. Martínez, A. Doncel-Giménez, J. Cerdá, J. Calbo, R. Rodríguez, J. Aragó, J. Crassous, E. Ortí, L. Sánchez, *J. Am. Chem. Soc.* **2021**, *143*, 13281–13291.
[43] S. Okuda, N. Ousaka, T. Iwata, R. Ishida, A. Urushima, N. Suzuki, S. Nagano, T. Ikai, E. Yashima, *J. Am. Chem. Soc.* **2022**, *144*, 2775–2792.
[44] M. L. Ślęczkowski, M. F. J. Mabesoone, P. Ślęczkowski, A. R. A. Palmans, E. W. Meijer, *Nat. Chem.* **2021**, *13*, 200–207.
[45] M. D. Preuss, S. A. H. Jansen, G. Vantomme, E. W. Meijer, *Isr. J. Chem.* **2021**, *61*, 622–628.
[46] J. S. Kang, S. Kang, J.-M. Suh, S. M. Park, D. K. Yoon, M. H. Lim, W. Y. Kim, M. Seo, *J. Am. Chem. Soc.* **2022**, *144*, 2657–2666.
[47] Y. Li, A. Hammoud, L. Bouteiller, M. Raynal, *J. Am. Chem. Soc.* **2020**, *142*, 5676–5688.
[48] N. J. Van Zee, M. F. J. Mabesoone, B. Adelizzi, A. R. A. Palmans, E. W. Meijer, *J. Am. Chem. Soc.* **2020**, *142*, 20191–20200.
[49] J. van Gestel, P. van der Schoot, M. A. J. Michels, *Macromolecules* **2003**, *36*, 6668–6673.
[50] J. van Gestel, P. van der Schoot, M. A. J. Michels, *J. Chem. Phys.* **2004**, *120*, 8253–8261.
[51] S. Díaz-Cabrera, Y. Dorca, J. Calbo, J. Aragó, R. Gómez, E. Ortí, L. Sánchez, *Chem. Eur. J.* **2018**, *24*, 2826–2831.
[52] Y. Wada, K. Shinohara, H. Asakawa, S. Matsui, T. Taima, T. Ikai, *J. Am. Chem. Soc.* **2019**, *141*, 13995–14002.
[53] E. E. Greciano, R. Rodríguez, K. Maeda, L. Sánchez, *Chem. Commun.* **2020**, *56*, 2244–2247.
[54] V. Ayzac, M. Dirany, M. Raynal, B. Isare, L. Bouteiller, *Chem. Eur. J.* **2021**, *27*, 9627–9633.
[55] S. Chen, K. Wang, Z. Geng, Y. Chen, X. Zheng, H. Wang, J. Zhu, *Polym. Chem.* **2019**, *10*, 4740–4745.
[56] M. Raynal, F. Portier, P. W. van Leeuwen, L. Bouteiller, *J. Am. Chem. Soc.* **2013**, *135*, 17687–17690.
[57] A. Desmarchelier, X. Caumes, M. Raynal, A. Vidal-Ferran, P. W. N. M. van Leeuwen, L. Bouteiller, *J. Am. Chem. Soc.* **2016**, *138*, 4908–4916.
[58] J. M. Zimbron, X. Caumes, Y. Li, C. M. Thomas, M. Raynal, L. Bouteiller, *Angew. Chem. Int. Ed.* **2017**, *56*, 14016–14019; *Angew. Chem.* **2017**, *129*, 14204–14207.
[59] Y. Li, X. Caumes, M. Raynal, L. Bouteiller, *Chem. Commun.* **2019**, *55*, 2162–2165.
[60] M. A. Martínez-Aguirre, Y. Li, N. Vanthuyne, L. Bouteiller, M. Raynal, *Angew. Chem. Int. Ed.* **2021**, *60*, 4183–4191; *Angew. Chem.* **2021**, *133*, 4229–4237.
[61] P. Aoun, A. Hammoud, M. A. Martínez-Aguirre, L. Bouteiller, M. Raynal, *Catal. Sci. Technol.* **2022**, *12*, 834–842.
[62] S. Allenmark, *Chirality* **2003**, *15*, 409–422.
[63] C. Deutsch, N. Krause, *Chem. Rev.* **2008**, *108*, 2916–2927.
[64] A. J. Jordan, G. Lalic, J. P. Sadighi, *Chem. Rev.* **2016**, *116*, 8318–8372.
[65] The slightly higher catalytic selectivities of copper-rich helices is also reflected by the higher slopes of the linear fitting of the *e.e.* versus g plots shown in Figure [MR2] .
[66] X. Lou, R. P. M. Lafleur, C. M. A. Leenders, S. M. C. Schoenmakers, N. M. Matsumoto, M. B. Baker, J. L. J. van Dongen, A. R. A. Palmans, E. W. Meijer, *Nat. Commun.* **2017**, *8*, 15420.
[67] Chiral defects present in supramolecular BTA helices formed in water are removed upon reaching the thermodynamic state, which is opposite to the behaviour observed in the present system, for which chiral defects appear over time: S. M. C. Schoenmakers, A. J. H. Spiering, S. Herziger, C. Böttcher, R. Haag, A. R. A. Palmans, E. W. Meijer, *ACS Macro Lett.* **2022**, *11*, 711–715.
[68] A. Desmarchelier, M. Raynal, P. Brocorens, N. Vanthuyne, L. Bouteiller, *Chem. Commun.* **2015**, *51*, 7397–7400.
[69] A. Desmarchelier, B. G. Alvarenga, X. Caumes, L. Dubreucq, C. Troufflard, M. Tessier, N. Vanthuyne, J. Idé, T. Maistriaux, D. Beljonne, P. Brocorens, R. Lazzaroni, M. Raynal, L. Bouteiller, *Soft Matter* **2016**, *12*, 7824–7838.
[70] X. Caumes, A. Baldi, G. Gontard, P. Brocorens, R. Lazzaroni, N. Vanthuyne, C. Troufflard, M. Raynal, L. Bouteiller, *Chem. Commun.* **2016**, *52*, 13369–13372.
[71] M. Raynal, Y. Li, C. Troufflard, C. Przybylski, G. Gontard, T. Maistriaux, J. Idé, R. Lazzaroni, L. Bouteiller, P. Brocorens, *Phys. Chem. Chem. Phys.* **2021**, *23*, 5207–5221.
[72] G. Vantomme, G. M. ter Huurne, C. Kulkarni, H. M. M. ten Eikelder, A. J. Markvoort, A. R. A. Palmans, E. W. Meijer, *J. Am. Chem. Soc.* **2019**, *141*, 18278–18285.

[73] F. Perlitius, A. Walczak, M. Čonková, G. Markiewicz, J. Harrowfield, A. R. Stefankiewicz, *J. Mol. Liq.* **2022**, *367*, 120511.
[74] D. Valigura, M. Koman, E. Ďurčanská, G. Ondrejovič, J. Mroziński, *J. Chem. Soc. Dalton Trans.* **1986**, *0*, 2339–2344.
[75] B. J. Edmondson, A. B. P. Lever, *Inorg. Chem.* **1965**, *4*, 1608–1612.
[76] P. J. M. Stals, P. A. Korevaar, M. A. J. Gillissen, T. F. A. de Greef, C. F. C. Fitié, R. P. Sijbesma, A. R. A. Palmans, E. W. Meijer, *Angew. Chem. Int. Ed.* **2012**, *51*, 11297–11301; *Angew. Chem.* **2012**, *124*, 11459–11463.
[77] Z. Shen, T. Wang, M. Liu, *Angew. Chem. Int. Ed.* **2014**, *53*, 13424–13428; *Angew. Chem.* **2014**, *126*, 13642–13646.
[78] J. Sun, Y. Li, F. Yan, C. Liu, Y. Sang, F. Tian, Q. Feng, P. Duan, L. Zhang, X. Shi, B. Ding, M. Liu, *Nat. Commun.* **2018**, *9*, 2599.
[79] Z. Shen, Y. Sang, T. Wang, J. Jiang, Y. Meng, Y. Jiang, K. Okuro, T. Aida, M. Liu, *Nat. Commun.* **2019**, *10*, 3976.
[80] F. V. Gruschwitz, F. Hausig, P. Schüler, J. Kimmig, S. Hoeppener, D. Pretzel, U. S. Schubert, S. Catrouillet, J. C. Brendel, *Chem. Mater.* **2022**, *34*, 2206–2217.
[81] E. Vereroudakis, M. Bantawa, R. P. M. Lafleur, D. Parisi, N. M. Matsumoto, J. W. Peeters, E. Del Gado, E. W. Meijer, D. Vlassopoulos, *ACS Cent. Sci.* **2020**, *6*, 1401–1411.
[82] S. Hafeez, F. R. Passanha, A. J. Feliciano, F. A. A. Ruiter, A. Malheiro, R. P. M. Lafleur, N. M. Matsumoto, C. van Blitterswijk, L. Moroni, P. Wieringa, V. L. S. LaPointe, M. B. Baker, *Biomater. Sci.* **2022**, *10*, 4740–4755.

Manuscript received: January 18, 2023
Accepted manuscript online: February 23, 2023
Version of record online: ■■, ■■

RESEARCH ARTICLE

Lower optical purities of supramolecular helical catalysts embedding a low fraction of "sergeants" is due to the aggregation of single helices through copper crosslinks.[MR1]

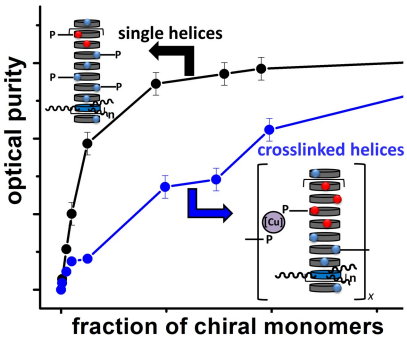

*Dr. A. Hammoud, Dr. Y. Li, Dr. M. A. Martínez-Aguirre, H. Kong, L. Dubreucq, C. Troufflard, Dr. L. Bouteiller, Dr. M. Raynal**